Integrating population-level and cell-based signatures for drug repositioning

Chunfeng He[1,2,#], Yue Xu[1,2,#], Yuan Zhou[3], Jiayao Fan[1,2], Chunxiao Cheng[1], Ran Meng[1], Lang Wu[4], Eric R. Gamazon[5,6], Dan Zhou[1,2]

[1]School of Public Health and the Second Affiliated Hospital, Zhejiang University School of Medicine, Hangzhou, China;

[2]The Key Laboratory of Intelligent Preventive Medicine of Zhejiang Province, Hangzhou, Zhejiang, China;

[3]Department of Biostatistics and Center for Quantitative Sciences, Vanderbilt University Medical Center, Nashville, TN, USA;

[4]Cancer Epidemiology Division, Population Sciences in the Pacific Program, University of Hawaii Cancer Center, University of Hawaii at Manoa, Honolulu, HI, USA

[5]Vanderbit Genetics Institute, Vanderbilt University Medical Center, Nashville, TN, USA;

[6]Data Science Institute, Vanderbilt University Medical Center, Nashville, TN, USA;

[#]equally contributed

[*]Corresponding to:

Dan Zhou: danzhou@zju.edu.cn

Eric Gamazon: egamazon@gmail.com

Highlights

- TReD is a genetics-informed framework that integrates population-level disease signatures and cell-based drug response profiles for drug repositioning.
- The effectiveness of TReD is demonstrated by identifying established and new therapeutic candidates for COVID-19 and type 2 diabetes.
- Single-gene (TWAS and coloc-SuSiE) and multi-target (TReD) drug repositioning approaches are integrated to enable a comprehensive therapeutic search.

Summary

Genetics-informed drug repositioning presents a streamlined and cost-efficient way to broaden therapeutic options. However, leveraging the full spectrum of molecular signatures remains underexplored. We introduce TReD (Transcriptome-informed Reversal Distance), integrating population-level disease signatures robust to reverse causality and cell-based drug-induced response profiles. TReD embeds the disease signature and drug profile in a high-dimensional normed space, quantifying the reversal potential of candidate drugs in a disease-related cell screen assay. For illustration, we apply TReD to COVID-19 and type 2 diabetes (T2D). We identify 37 potential drugs against COVID-19, over 70% (27/37) with prior associations, and eight supported by clinical trials. For T2D, we observe reversal signals for 86 compounds on multiple disease signatures, with more than 40% supported by published literature. In summary, we propose a comprehensive genetics-anchored framework integrating population-level signatures and cell-based screens that can accelerate the search for new therapeutic strategies.

Graphical abstract

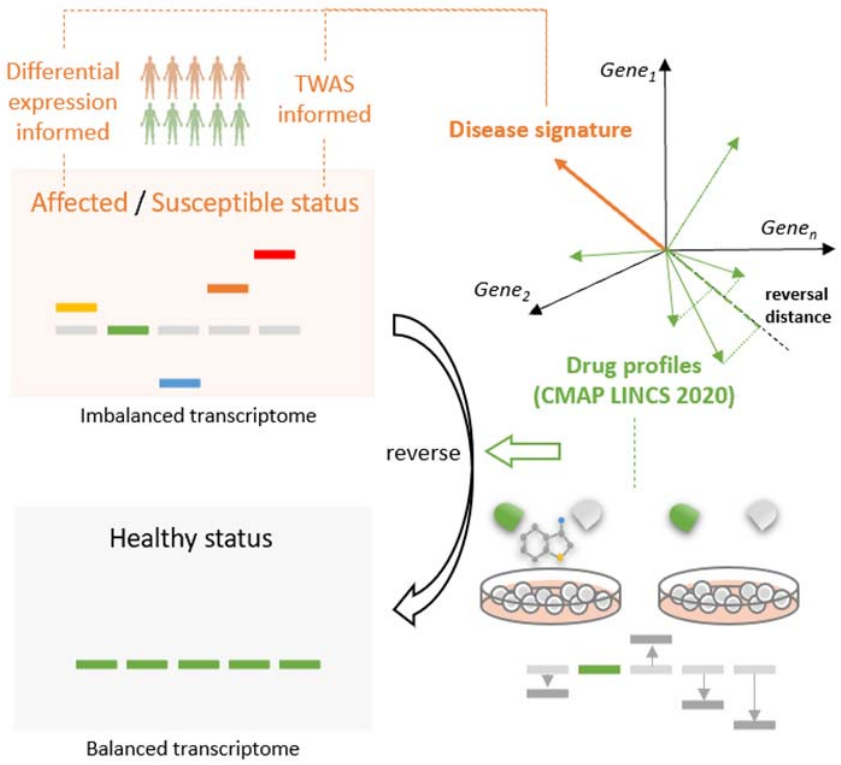

Key words

Drug repositioning; signature matching; TWAS; reversal distance; COVID-19; T2D

Introduction

The conventional model of drug development is commonly perceived as a time-consuming and costly endeavor, with recent statistics revealing that it typically spans 10-15 years, and necessitates a financial investment exceeding $1.3 billion to introduce a new drug to the market[1,2]. In contrast, drug repositioning is a cost-effective strategy to extend the utility of existing drugs and offer shorter pathways to approval for new therapeutic indications, since the safety has already been confirmed in preclinical and the first two stages of clinical trials.

Leveraging genetic evidence of disease association helps to address this challenge since empirical data have shown that drug targets with genetic support are more likely to be successful[3,4]. Genome-wide association analysis (GWAS) and Transcriptome-wide association analysis (TWAS) / Proteome-wide association study (PWAS) are powerful genetic tools to predict drug repurposing candidates. For example, the genome-wide significant association between *TYK2* and critical illness in COVID-19[5], directly led to the drug repurposing of baricitinib, which has demonstrated clear therapeutic benefit in subsequent clinical trials[6-8].

However, drug repositioning focused on a single gene target may be blind to molecular processes that are inevitably connected, through complex networks, with multiple levels of the organizational hierarchy of biological systems[9]. The growing evidence for polypharmacology entails the adoption of experimental and computational multitarget approaches[10,11]. Utilizing the transcriptome at the cellular level, a method that performs an inverse pattern-matching alignment of disease signatures and drug profiles[12,13] posits that, for a given disease signature comprising a set of genes with altered up and down-regulation, a drug that reverses the disease-associated gene expression changes holds therapeutic potential for the disease. Most existing approaches rely on differential gene expression

(DGE) to generate a list of prioritized genes. However, the transcriptome perturbations identified by DGE are challenging to interpret as molecular consequences or causes of disease, with one recent study claiming a higher likelihood of implicated genes being of the former class[14]. Consequently, methodologies grounded in DGE analysis inherently struggle to determine the direction of pharmacological effect (therapeutic or harmful) on disease when lacking the context of a known disease pathogenesis. In contrast, genetically-anchored TWAS minimizes the problem of reverse causality. Patrick Wu et al. applied the PrediXcan[15] models to find drug repurposing candidates using the Integrative Library of Integrated Network-based Cellular Signatures (iLINCS) platform[16]. The latest release (CMAP LINCS 2020) of this platform contains over 3 million gene expression profiles with > 80,000 perturbations and > 200 cell lines. The resource is roughly a 3-fold expansion relative to the previous version (2017)[17]. Methodologically, previous approaches (for example, a widely adopted nonparametric pattern-matching strategy based on the Kolmogorov−Smirnov (KS) statistic[18,19]) do not fully consider the pattern of alignment between the (transcript)omic features of drug induction and disease susceptibility – including, explicitly, genetically-determined risk – within a multitarget or polygenic framework. In summary, a genetics-informed omics-based repurposing framework that addresses critical methodological gaps is needed.

We developed Transcriptome-informed Reversal Distance (TReD) to integrate cell-based drug profiles (CMAP LINCS 2020) and population-level disease signatures (TWAS and DGE) to identify drug repurposing candidates. For illustration, we applied the framework to search for drug repurposing candidates for COVID-19 and T2D.

Results

An overview of the study

Genetics-informed single-gene matching and omics profile-based signature matching are two promising approaches used in drug repurposing[20], with diverse types of omics data providing a valuable opportunity[21]. In this study, we integrated these two approaches, leveraging transcriptome data to identify potential drug repurposing candidates (Figure 1). A single gene-based approach that combines TWAS and colocalization analysis (coloc-SuSiE) detects genes associated with disease (Figure 1a, Figure S1). Subsequently, drugs targeting these genes are prioritized as candidate therapeutics. For the multi gene-based approach, we developed TReD, integrating TWAS- and DGE-derived disease signatures and cell-based drug profiles (CMAP LINCS 2020) (Figure 1b, Figure S1). In this study, we focused primarily on the drug profile data arising from small-molecule perturbations in immune-related cells and blood glucose metabolism-related tissues for the specific TReD applications to COVID-19 and T2D, respectively. TReD is based on transcriptome signature matching, which relies on the signature reversion principle[22]. In contrast to previous transcriptome signature pattern-matching studies[23], we calculated the reversal potential, using an easily interpretable metric, of the cell-based drug signature on the population-level disease profile, including genetically-determined risk (**STAR Methods**). The approximate expressions for the mean and variance of the metric are derived in STAR Methods. Intuitively, the reversal distance quantifies the drug's potential in reversing the disease-associated gene expression, using a metric that is scale-invariant and directionality-focused. To conduct hypothesis testing and evaluate the statistical significance, we employed a permutation approach.

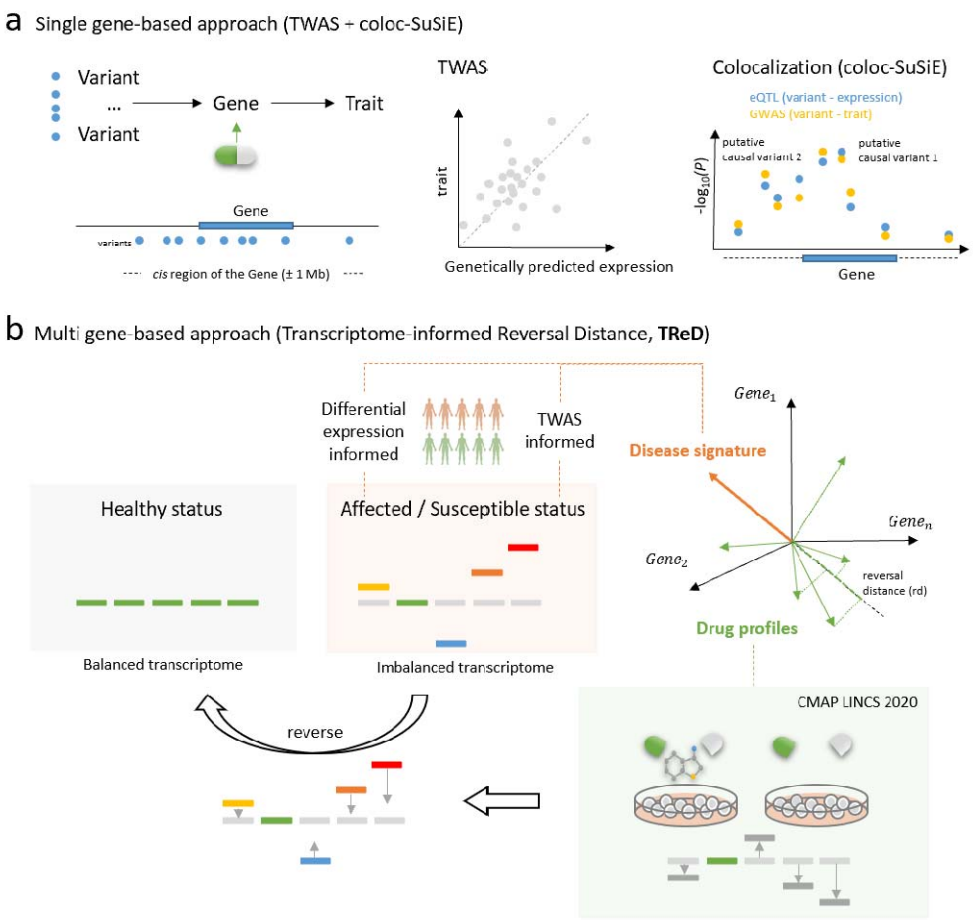

Figure 1. The framework overview. (a) Single gene-based approach integrates TWAS (e.g., PrediXcan) and colocalization analysis (e.g., coloc-SuSiE). (b) Multi-gene-based approach TReD (Transcriptome-informed Reversal Distance) utilizes DGE- and TWAS-derived population-level gene expression profiles as disease signatures, reflecting affection status and germline susceptibility, respectively. By embedding the population-level disease signatures (orange vector) and the cell-based drug profiles (green vectors) in the same high-dimensional space, the reversal distance (*rd*) is estimated for each drug. A permutation test is used to estimate the statistical significance of the reversal distance (**STAR★Methods**).

Single-target drug repositioning using TWAS and coloc-SuSiE

We performed a TWAS to identify the associations between gene expression and phenotype. This was achieved by training gene expression prediction models using a reference panel and applying the models to GWAS of COVID-19 severity and T2D. For this analysis, we used data from Genotype-Tissue Expression (GTEx) v8, focusing on tissues relevant to COVID-19 / T2D, namely whole blood, lung, lymphocytes, and spleen samples[24] / visceral adipose, liver, pancreas, and skeletal muscle. Genes that survived Bonferroni correction for each tissue were considered significant (Figure 2, Table S1). For TWAS results that passed the significance threshold after accounting for multiple testing, we performed coloc/coloc-SuSiE. We considered that the signals of eQTL and GWAS were colocalized if the maximum posterior probability of colocalization (i.e., PP.H4 for coloc or coloc-SuSiE) was greater than or equal to 0.85. The results of coloc can be found in Table S2 and coloc-SuSiE in Table S3. We further examined which of the prioritized disease-related genes are possible drug targets, thereby identifying potential therapeutic drugs for the disease. Drug target genes were defined using public databases, including DrugBank[25], The Drug Gene Interaction Database (DGIdb)[26] and the Therapeutic Target Database (TTD)[27].

For COVID-19 severity, we identified 34, 45, 27, and 43 significant genes in blood, lung, lymphocytes, and spleen, respectively in TWAS results. Nine genes showed significance across four tissues. Notably, *tyrosine kinase 2* (*TYK2)* was significant in all tissues with a concordant positive effect, which means that an increased expression of *TYK2* is associated with an increased risk of severe COVID-19. *TYK2* is an intracellular kinase belonging to the Janus kinase (JAK) family, which plays a pivotal role in the Janus Kinase–Signal Transducer and Activator of Transcription (JAK-STAT)

pathway. Previous studies have also revealed that high expression of *TYK2* and host-driven inflammatory lung injury are related to life-threatening COVID-19[5,28]. *RAB2A* also shows a positive effect in TWAS results of the four tissues. The gene is required for SARS-CoV-2 replication[29] and it has been reported that higher expression of this gene is associated with worse COVID-19 outcome[30], aligning with our findings.

In the four analyzed tissues, we identified a total of 28 unique genes post coloc/coloc-SuSiE (Figure S2), among these genes, 50% (14/28) have been reported to be associated with COVID-19 (*DPP9*[31,32], *WNT3*[33,34], *ABO*[35,36], *NAPSA*,[37] *GSDMB*[38,39], *RAB2A*[30], *OAS1*[40], *OAS3*[5], *LRRC37A2*[41], *MAPT*[33], *FUT2*[42,43], *IKZF3*[44], *ICAM5*[42,45], *CCR9*[35,46]). *CCR9* and *MAPT* are druggable genes. Drugs such as Docetaxel and Astemizole, which target *MAPT*, had COVID-19-related support. Docetaxel was noted to have the potential to bind the active site residues of SARS-CoV-2 RdRP, and exert antiviral effects by inhibiting the activity of SARS-CoV-2 RdRP[47]. Astemizole is an antihistamine medication that is used to relieve allergy symptoms. Wang X, et al. found that astemizole can antagonize ACE2 and inhibit the entry of SARS-COV-2 spike pseudovirus into ACE2-expressed HEK293T cells (ACE2hi cells)[48]. This highlights astemizole as a potential drug candidate that can be repurposed in anti-coronavirus therapies.

For T2D, we performed TWAS and coloc/coloc-SuSiE in several disease-relevant tissues: visceral adipose, liver, skeletal muscle, and pancreas. In total, 86 genes were identified by both TWAS coloc/coloc-SuSiE in these tissues. We further investigated their associations with T2D in the Type 2 Diabetes Knowledge Portal[49]. Among the 86 genes, ten have been classified as potential T2D effectors, including well-established genes such as *IRS1*. Insulin receptor substrate-1 (IRS1) is a substrate of the insulin receptor tyrosine kinase and has a central role in the insulin-stimulated signal transduction pathway.

We also identified T2D-associated genes *PTH1R* and *NOTCH2*, which are druggable genes. *PTH1R* showed a negative effect on T2D in visceral adipose. Teriparatide and abaloparatide function as agonists of the *PTH1R*, suggesting potential therapeutic value for T2D. Of note, TPTD has been shown to be associated with improved glucose metabolic control in subjects with glucocorticoid-induced osteoporosis compared to treatment with bisphosphonates[50]. *NOTCH2* showed a negative effect in both the liver and visceral adipose tissue, but drugs targeting the gene such as nirogacestat and rg-4733 are identified as inhibitors.

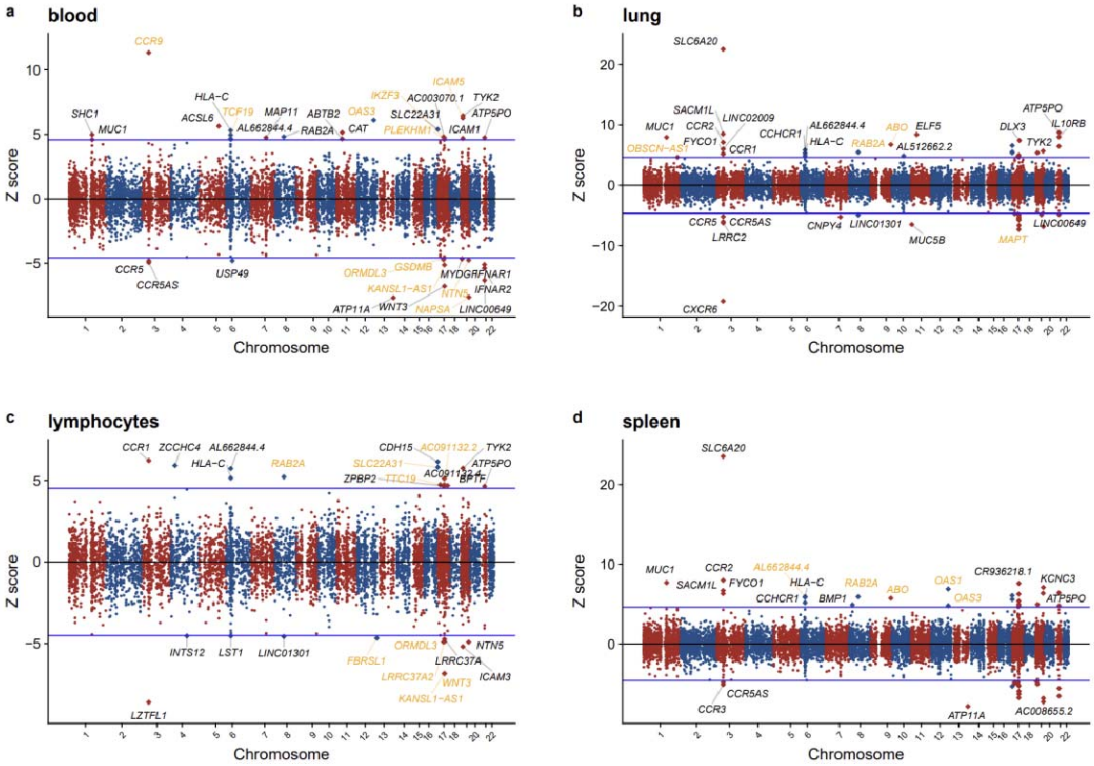

Figure 2. TWAS and colocalization analysis for COVID-19. Manhattan plots of TWAS results for COVID-19 severity in whole blood (a), lung (b), lymphocytes (c), and spleen (d), respectively. The Z-scores for TWAS are shown. Z-score > 0 denotes a gene for which increased genetically-determined expression is associated with COVID-19 severity. The highlighted genes survived multiple testing

corrections (over or below the blue lines) for the number of genes tested. Genes that further pass the significance threshold from the colocalization analysis are colored gold.

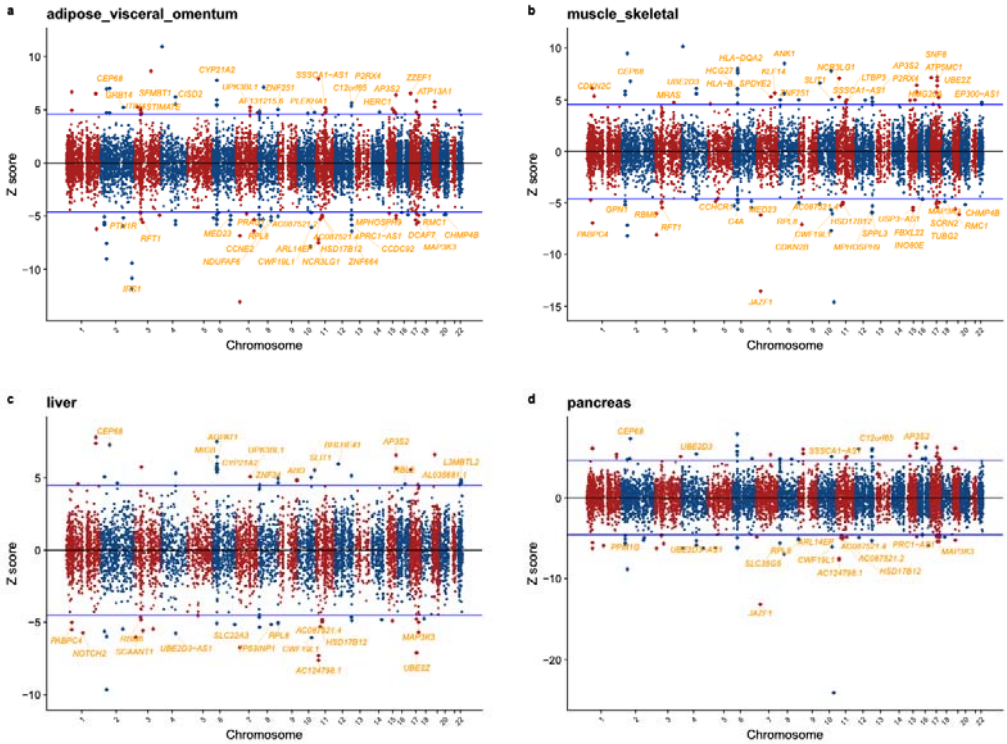

Figure 3. TWAS and colocalization analysis for T2D. Manhattan plots of TWAS results for T2D in visceral adipose (a), skeletal muscle (b), liver (c), and pancreas (d), respectively. The Z-scores for TWAS are shown. Z-score > 0 denotes a gene for which increased genetically-determined expression is associated with T2D. The highlighted genes survived multiple testing corrections (over or below the blue lines) for the number of genes tested. Genes that further pass the significance threshold from the colocalization analysis are colored gold.

Multi-target drug repositioning using TReD

We applied the TReD framework to identify potential drug repurposing candidates for COVID-19

and T2D. We sought to identify significant reversal effects of the cell-based drug profiles on the population-level disease signatures at the level of the transcriptome (**STAR Methods**). In addition to the four TWAS-derived disease signatures, we included three DGE-based disease signatures. The detailed results of TReD can be found in Table S4. A significant drug was defined by a large reversal distance (i.e., over 2 standard deviations from the mean across the tested drugs) and $P < 0.05$ in a permutation test (**STAR Methods**).

For COVID-19, drugs that met both the reversal distance threshold and statistical significance for either TWAS or DGE-based disease signature in at least two cell lines were considered as potential candidates. We obtained 263 drug profiles meeting the criteria for any of the seven disease signatures (Table S5). Here, we focused on the 37 drugs that showed significant reversal effects against at least four disease signatures (Figure 3). Table 1 provides an overview of the 37 drugs, including the reversal distance values across the different disease signatures and whether there is any prior evidence linking them to COVID-19 and/or clinical studies for the treatment of COVID-19. Notably, more than 70% of the drugs (27/37) have been reported to be related to COVID-19, and eight drugs have ongoing/completed clinical trials.

It is worth noting that over 40% of the candidates are immunomodulatory drugs, especially JAK inhibitors. Baricitinib, significantly reversing four disease signatures (Figure 4b), is a JAK1/2 and TYK2 inhibitor, and has been approved for the treatment of COVID-19 by FDA in 2022. Ruxolitinib significantly reversed all seven disease signatures (Figure 4a). Case reports or small cases series have reported that Ruxolitinib might be helpful in combating COVID-19[51-53]. The RUXCOVID[54] and phase 3 RUXCOVID-DEVENT[55] study showed no statistically significant improvement in mortality through day 29 compared with placebo. However, in the RUXCOVID-DEVENT study, when US

study participants were analyzed separately, significant benefits were observed[55], indicating effectiveness.

Enzastaurin was found to be effective in reversing six disease signatures (Figure 5). Enzastaurin is an investigational agent for the treatment of relapsed glioblastoma multiforme (GBM). Enzastaurin was designed to selectively inhibit PKC-beta and other kinases involved in cell proliferation and survival. SARS-CoV can activate the PKC members[56], suggesting that these might be involved in SARS-CoV-2 infection. An *in vitro* study revealed that bisindolylmaleimide IX, a PKC inhibitor, targets the viral protease 3CLpro[57]. Another study found that several inhibitors of protein kinases C (PKCs) including enzastaurin decrease the replication of SARS-CoV-2 in cultured cells[58]. The evidence above indicates that enzastaurin is a potential therapeutic agent against SARS-CoV-2. We also investigated the drugs that are *positively* correlated with the disease signatures with a high cosine similarity. A few such top-ranked drugs (including testosterone[59] and otamixaban[60]) were also supported by published studies as potential treatment options. This scenario may arise, for example, when a disease signature targeted by such a drug lies in a co-expression network with another disease signature whose net reversal is a potential therapeutic option. This result indicates that, in reality, the biological system operates in a much more complex fashion.

For T2D, eleven compounds exhibited significant reversal effects on three disease signatures. Four of the eleven compounds showed evidence of a protective effect on T2D. Caffeine was effective in reversing one TWAS and two DGE signatures, indicating its molecular-level protective influence on T2D. Epidemiological studies report a consistent inverse linear association between coffee consumption and T2D[61]. A recent Mendelian randomisation study also revealed that elevated concentrations of caffeine in the plasma have potential causal effects on type 2 diabetes[62]. Further clinical study is warranted to

investigate the potential of caffeine towards reducing the burden of diabetes. Erlotinib is another promising drug. In a T2D mouse model, Erlotinib treatment preserved pancreas function and increased glucose tolerance and insulin sensitivity[63]. In addition to the eleven compounds, we identified another 75 compounds as potential candidates for at least two T2D disease signatures (one TWAS and one DGE, detailed results can be found in Table S6). The top 50% of the 75 compounds with the highest cumulative reversal distances across multiple conditions are presented in Figure 5. Remarkably, more than half of the drugs have been previously reported as potential options for the prevention or treatment for T2D and its related complications. Imatinib exhibited a notably elevated reversal distance, ranking second. Imatinib can improve insulin sensitivity and maintain glucose homeostasis[64]. It has been established that imatinib mesylate reduces endoplasmic reticulum stress and induces remission of diabetes in db/db mice[65]. Pimozide ranked fourth in the reversal distance ordering. A previous study indicated that pimozide alleviates hyperglycemia in diet-induced obesity by inhibiting skeletal muscle ketone oxidation[66]. Deferasirox, the first orally administered iron chelator approved by FDA, showed significant reversal effect on a TWAS signature in pancreas and consistently on the DGE signature in islets. Although there are currently no reports of deferasirox being used for diabetes, high iron is a risk factor for T2D and affects most of its cardinal features[67]. Collectively, our findings correspond to a variety of drugs that exhibit therapeutic evidence for T2D, underscoring the predictive performance of TReD.

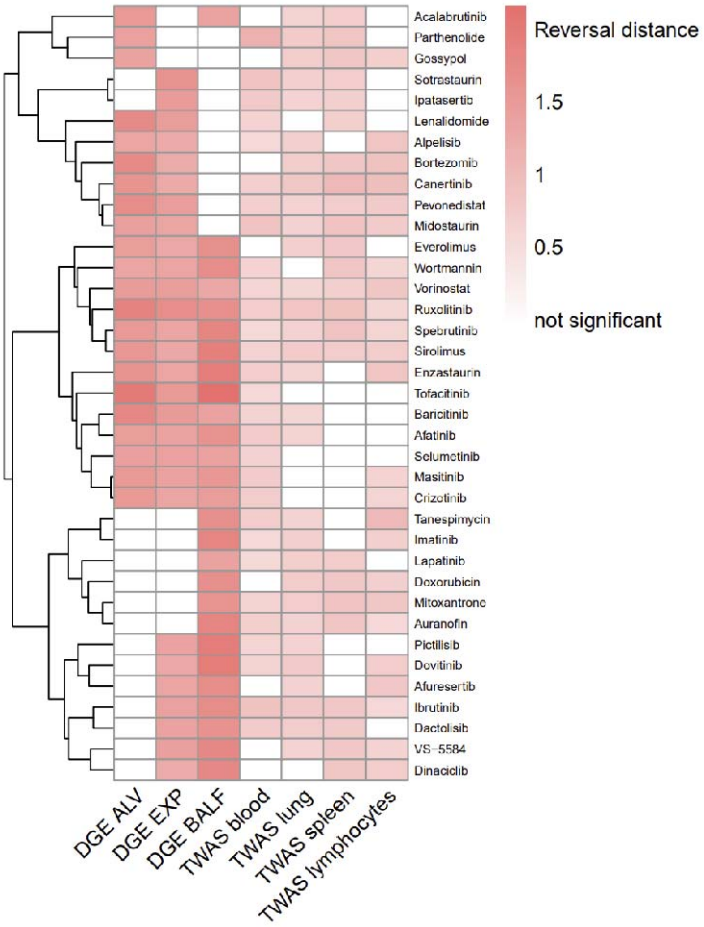

Figure 4. Drug repositioning candidates with potential reversal effect on the disease signatures from DGE and TWAS. In total, 37 drugs were found by our Transcriptome-informed Reversal Distance (TReD) framework (**STAR★Methods**) to have a potential reversal effect on COVID-19 as indicated by at least four of the seven tested transcriptome-based disease signatures (x-axis). The heatmap shows the reversal distance for each drug response profile / disease signature pair. Blank cells denote "not significant" in the permutation test (the information of significance can be found in Table S4). Hierarchical clustering was performed on the drug response profile (y-axis). The source data for the disease signatures, including TWAS (four tissue/cell types) and DGE (ALV, EXP, and BALF), are described in STAR★Methods.

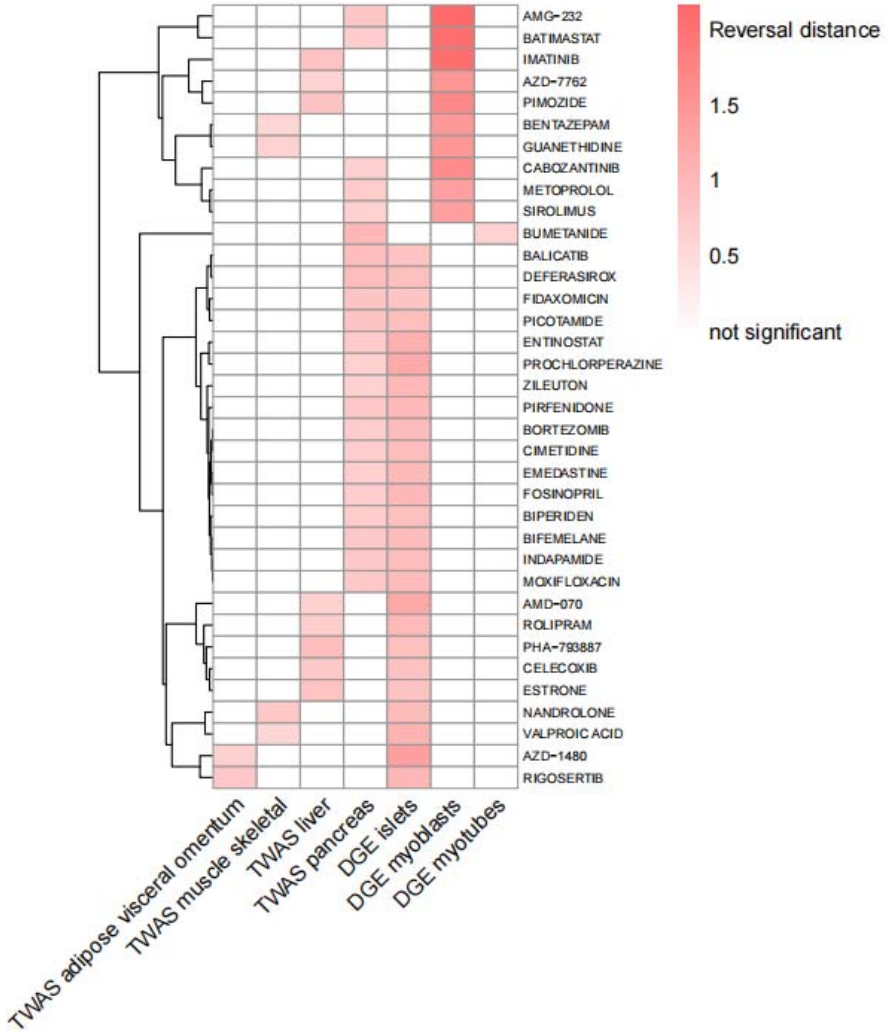

Figure 5. Drug repositioning candidates with potential reversal effect on the disease signatures from DGE and TWAS. In total, 36 drugs were found by our Transcriptome-informed Reversal Distance (TReD) framework (**STAR★Methods**) to have a potential reversal effect on T2D as indicated by two of the seven tested transcriptome-based disease signatures (x-axis). The heatmap shows the reversal distance for each drug response profile / disease signature pair. Blank cells denote "not significant" in the permutation test (the information of significance can be found in Table S4). Hierarchical clustering was performed on the drug response profile (y-axis). The source data for the

disease signatures, including TWAS (four tissue/cell types) and DGE, are described in STAR★ Methods.

Table 1. DrugBank annotations for drugs with significant reversal effects on at least four disease signatures for COVID-19.

		Reversal distance for each of the disease signatures							Evidence for COVID-19	Evidence for clinical trials
Drug Hit	Description	DGE ALV	DGE EXP	DGE BALF	TWAS blood	TWAS lung	TWAS spleen	TWAS lymphocytes		
Wortmannin	PI3Ks inhibitor	1.350	1.347	1.699	0.653	n.s.	0.829	0.603	Yes[68]	No
VS-5584	Antineoplastic	n.s.	1.426	1.784	n.s.	0.644	0.794	0.640	Yes[69]	No
Vorinostat	Antineoplastic	1.465	1.458	1.305	0.632	0.597	0.700	0.813	Yes[70]	No
Tofacitinib	Antineoplastic and Immunomodulating	1.991	1.518	2.159	0.583	n.s.	n.s.	n.s.	Yes[71]	Yes
Tanespimycin	Antitumor antibiotics	n.s.	n.s.	1.665	0.740	0.653	n.s.	1.026	No	No
Spebrutinib	Immunomodulator	1.507	1.339	1.828	0.554	0.674	0.860	0.624	Yes[72]	No
Sotrastaurin	Immunosuppressant	n.s.	1.625	n.s.	0.855	0.720	0.727	n.s.	Yes[58]	No
Sirolimus	Immunosuppressant	1.531	1.299	1.939	0.653	0.743	0.731	0.733	Yes[73]	Yes
Selumetinib	Antineoplastic	1.426	1.406	1.411	0.667	n.s.	n.s.	n.s.	Yes[74]	No
Ruxolitinib	Antineoplastic and Immunomodulating	1.871	1.685	1.666	0.722	0.845	0.878	0.592	Yes[75]	Yes
Pictilisib	PI3K inhibitors	n.s.	1.377	1.944	0.615	0.636	n.s.	n.s.	No	No

Pevonedistat	Antineoplastic	1.686	1.450	n.s.	0.709	0.650	0.732	0.785	No	No
Parthenolide	Anti-Inflammatory	1.403	n.s.	n.s.	1.138	0.753	0.841	n.s.	Yes[76]	No
Mitoxantrone	Chemotherapy drugs	n.s.	n.s.	1.599	0.648	0.729	0.852	0.821	Yes[77]	No
Midostaurin	Antineoplastic	1.438	1.325	n.s.	0.863	0.672	0.853	0.748	No	No
Masitinib	Antineoplastic and Immunomodulating	1.511	1.372	1.529	0.750	n.s.	n.s.	0.639	Yes[78]	Yes
Lenalidomide	Antineoplastic and Immunomodulating	1.750	1.441	n.s.	0.646	n.s.	0.714	n.s.	Yes[79]	No
Lapatinib	Antineoplastic	n.s.	n.s.	1.357	0.541	0.709	0.733	n.s.	Yes[80]	No
Ipatasertib	Antineoplastic	n.s.	1.478	n.s.	0.768	0.654	0.708	n.s.	No	No
Imatinib	Antineoplastic	n.s.	n.s.	1.814	0.552	0.700	n.s.	0.719	Yes[81]	Yes
Ibrutinib	Antineoplastic	n.s.	1.413	1.685	0.876	0.793	0.789	0.581	Yes[72]	Yes
Gossypol	Polyphenolic compounds	1.374	n.s.	n.s.	n.s.	0.738	0.824	0.711	Yes[82]	No
Everolimus	Antineoplastic	1.457	1.288	1.648	n.s.	0.698	0.797	n.s.	Yes[83]	No
Enzastaurin	Antineoplastic	1.616	1.346	1.957	0.738	0.642	n.s.	0.840	Yes[58]	No
Doxorubicin	Chemotherapy drugs	n.s.	n.s.	1.660	n.s.	0.730	0.798	0.685	Yes[84]	No
Dovitinib	Multi-targeted kinase inhibitor	n.s.	1.304	1.964	0.652	0.782	n.s.	0.737	No	No
Dinaciclib	Antineoplastic	n.s.	1.236	1.800	n.s.	n.s.	0.816	0.738	Yes[85]	No
Dactolisib	Antineoplastic	n.s.	1.363	1.629	0.761	0.732	0.772	n.s.	Yes[86]	No
Crizotinib	Antineoplastic	1.513	1.318	1.459	0.720	n.s.	n.s.	0.625	Yes[87]	No
Canertinib	Antineoplastic	1.613	1.253	n.s.	0.687	0.801	1.029	0.957	No	No
Bortezomib	Antineoplastic	1.766	1.241	n.s.	n.s.	0.734	0.826	0.883	Yes[88]	No
Baricitinib	Immunosuppressant	1.767	1.493	1.393	0.633	0.594	n.s.	n.s.	Yes[8]	Yes

Auranofin	Antiinflammatory and Antirheumatic	n.s.	n.s.	1.815	0.715	0.664	0.844	0.588	Yes[89]	No
Alpelisib	Antineoplastic	1.319	1.249	n.s.	0.582	0.711	n.s.	0.840	No	No
Afuresertib	Akt inhibitor	n.s.	1.334	1.680	n.s.	0.669	n.s.	0.794	No	No
Afatinib	Antineoplastic	1.442	1.369	1.628	0.744	0.641	n.s.	n.s.	No	No
Acalabrutinib	Antineoplastic	1.526	n.s.	1.355	n.s.	0.650	0.722	n.s.	Yes[90]	Yes

The estimated reversal distance is shown. N.s. denotes not significant in the permutation test. The source data for the disease signatures, including TWAS (four tissue/cell types) and DGE (ALV, EXP, and BALF), are described in STAR Methods.

Table 2. DrugBank annotations for drugs with significant reversal effects on two disease signatures for T2D.

		Reversal distance for each of the disease signatures							Evidence for T2D	Evidence for clinical trials
Drug Hit	Description	DGE islets	DGE myoblasts	DGE myotubes	TWAS adipose	TWAS muscle	TWAS liver	TWAS pancreas		
AMG-232	Antineoplastic	n.s	2.452	n.s	n.s	n.s	n.s	0.802	No	No
Batimastat	Antineoplastic	n.s.	2.063	n.s	n.s.	n.s	n.s	0.715	Yes[91]	No
Imatinib	Tk inhibitor	n.s	2.094	n.s	n.s	n.s	0.841	n.s	Yes[64]	No
AZD-7762	Chk inhibitor	n.s	1.489	n.s	n.s	n.s.	0.628.	n.s.	No	No
Pimozide	Antipsychotic	n.s.	1.692	n.s	n.s	n.s	0.830	n.s	Yes[66]	No
Bentazepam	Antipsychotic	n.s	1.448	n.s	n.s	0.586	n.s	n.s	No	No
Guanethidine	Antihypertensive drug	n.s.	1.463	n.s.	n.s	0.652	n.s	n.s.	Yes	No

Cabozantinib	Antineoplastic	n.s	1.657	n.s	n.s	n.s	n.s	0.634	Yes[92]	No
Metoprolol	Antiarrhythmic	n.s	1.371	n.s	n.s	n.s.	n.s.	0.375.	Yes[93]	No
Sirolimus	immunosuppressant	n.s	1.366	n.s	n.s	n.s	n.s	0.651	No	No
Bumetanide	Cardiovascular Agents	n.s.	n.s	0.620	n.s	n.s	n.s.	1.020.	Yes[94]	No
Balicatib	CTSK inhibitor	0.845	n.s	n.s.	n.s	n.s	n.s	0.927	No	No
Deferasirox	Iron Chelating Agents	0.906	n.s.	n.s.	n.s	n.s	n.s	0.933.	No	No
Fidaxomicin	Anti-Infective Agents	0.810	n.s.	n.s	n.s	n.s	n.s	0.811	No	No
Picotamide	Antiplatelet Agents	0.901	n.s	n.s.	n.s	n.s	n.s	0.837	Yes[95]	No
Entinostat	Antineoplastic	1.121	n.s	n.s	n.s	n.s.	n.s.	0.731	Yes[96]	No
Prochlorperazine	Antipsychotic Agents	1.202	n.s	n.s.	n.s	n.s.	n.s	0.652	No	No
Zileuton	Anti-Inflammatory Agents	1.020	n.s.	n.s	n.s	n.s	n.s	0.652	Yes[97]	No
Pirfenidone	Antifibrotic Agents	1.003	n.s	n.s.	n.s	n.s	n.s	0.779	No	No
Bortezomib	Antineoplastic	0.947	n.s.	n.s	n.s	n.s	n.s.	0.711	Yes[98]	No
Cimetidine	Anti-Ulcer Agents	0.931	n.s	n.s	n.s	n.s	n.s	0.704	No	No
Emedastine	Anti-Allergic Agents	0.961	n.s.	n.s.	n.s.	n.s	n.s	0.692	No	No
Fosinopril	ACE Inhibitors	0.986	n.s	n.s	n.s.	n.s	n.s	0.710	No	No
Biperiden	Anticholinergic Agents	0.891	n.s	n.s	n.s	n.s	n.s.	0.737	No	No
Bifemelane	Antidepressive Agents	0.946	n.s.	n.s	n.s.	n.s	n.s	0.777	No	No
Indapamide	Antihypertensive Agents	0.934	n.s	n.s	n.s	n.s	n.s.	0.747	Yes[99]	Yes
Moxifloxacin	Anti-Infective Agents	0.941	n.s	n.s	n.s.	n.s.	n.s	0.759	Yes[100]	Yes
AMD-070	CXCR4 antagonist	1.231	n.s	n.s	n.s	n.s	0.645	n.s.	No	No

Rolipram	Antidepressive Agents	0.964	n.s	n.s	n.s	n.s.	0.697.	n.s	Yes[101]	No
PHA-793887	CDK inhibitor	0.886	n.s	n.s.	n.s	n.s	0.930	n.s	No	No
Celecoxib	Anti-Inflammatory Agents	0.871	n.s	n.s.	n.s.	n.s	0.751	n.s	Yes[102]	No
Estrone	etosteroids	0.832	n.s	n.s	n.s	n.s	0.835	n.s.	No	No
Nandrolone	Gonadal Hormones	0.944	n.s.	n.s	n.s	0.746	n.s	n.s	Yes[103]	No
Valproic acid	Anti-epileptic Agent	1.0568	n.s	n.s.	n.s	0.565	n.s.	n.s	Yes[104]	No
AZD-1480	JAK inhibitor	1.353	n.s	n.s	0.666	n.s	n.s	n.s	Yes[105]	No
Rigosertib	Protein Kinase Inhibitors	1.023	n.s	n.s	n.s	0.767	n.s.	n.s.	No	No

The estimated reversal distance is shown. N.s. denotes not significant in the permutation test. The source data for the disease signatures, including TWAS (four tissue/cell types) and DGE (islets, myoblasts, and myotubes), are described in STAR Methods.

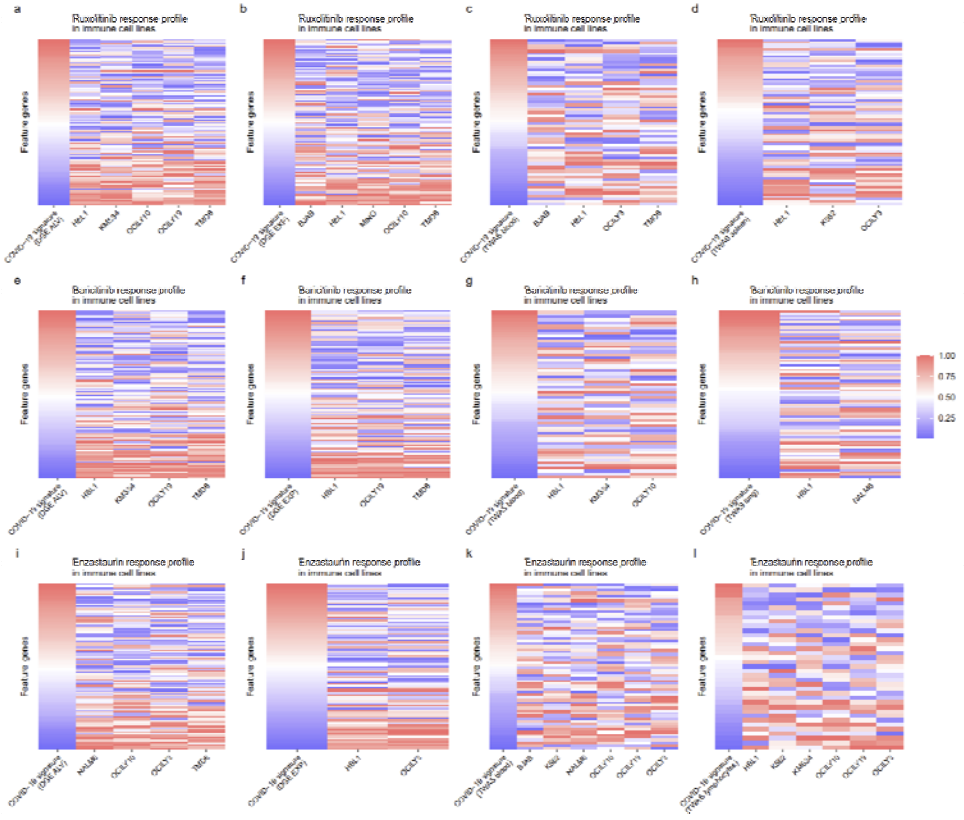

Figure 6. TReD-identified relationships between COVID-19 signatures and drug profiles. The potential reversal effects of Ruxolitinib (a-d), Baricitinib (e-h), and Enzastaurin (i-l), which were identified against at least four disease signatures of COVID-19, are visualized using a heatmap. Taking (a) as an example, the first column in the heatmap represents differential gene expression (DGE) from the ALV dataset gene expression disease signature ranked by fold change. Red and blue denote higher and lower expressed in affected samples, respectively. The remaining columns represent gene expression changes after Ruxolitinib treatment in immune cells. For drugs with multiple significant profiles, the drug profiles (e.g., different time points after treatment) with the largest reversal distance are presented. The source data for the disease signatures, including TWAS (four tissue/cell types) and DGE (ALV and EXP), are described in STAR★Methods.

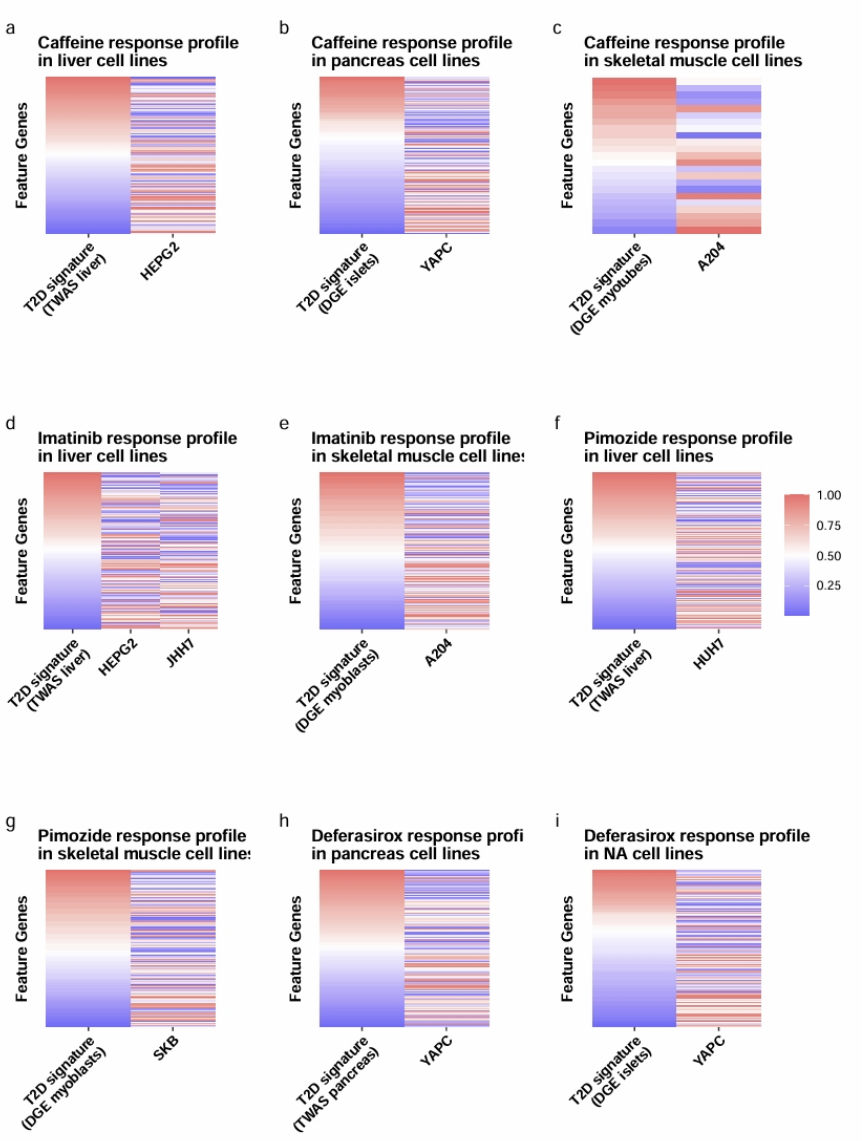

Figure 7. TReD-identified relationships between T2D signatures and drug profiles. The potential reversal effects of Caffeine (a-c), Imatinib (d-f), and Pimozide (g-i), which were identified against two disease signatures of T2D, are visualized using a heatmap. Taking (a) as an example, the first column in the heatmap represents the transcriptome-wide association analysis (TWAS) derived disease signature in liver ranked by fold change. Red and blue denote higher and lower expressed in affected samples, respectively. The remaining columns represent gene expression changes after Caffeine

treatment in liver cells. For drugs with multiple significant profiles (e.g., different time points after treatment), the drug profiles with the largest reversal distance are presented. The source data for the disease signatures, including TWAS (four tissue/cell types) and DGE, are described in STAR★ Methods.

Discussion

We developed a framework to identify potential drug repurposing candidates, incorporating population-level disease signatures using TWAS/DGE and cell-based drug-induced transcriptome responses. To demonstrate the effectiveness of this framework, we applied it to the up-to-date GWAS for COVID-19 and T2D. In our quest to uncover the transcriptome signatures relevant to COVID-19 using TWAS, we identified the *TYK2*, which exhibited a clear and substantial association with COVID-19 severity. For T2D, we identified *IRS1* and *GRB14*, which have been proven to play a crucial role in the development and progression of diabetes.

Using the proposed multi-target approach TReD, the screening results indicated a significant correlation between the potential candidates and the associated diseases. For COVID-19, nearly half (16/37) of the identified drugs were categorized as immunotherapeutic agents. Notably, all sixteen drugs have been studied in the context of COVID-19. SARS-CoV-2 infection can induce dysfunctional immune responses and aggressive inflammatory responses that are often associated with severe manifestations[106,107]. The Janus kinase (JAK)-signal transducer and activator of transcription (STAT) pathway is crucial for the intracellular signaling of numerous cellular processes, playing an essential role in immune-mediated inflammatory diseases. Furthermore, JAK-STAT activation

promotes senescence of SARS-CoV-2 infected cells, which amplifies inflammation[108]. JAK inhibition prevents downstream phosphorylation and hence activation of STAT. Several meta-analysis studies have reported the safety and efficacy of JAK inhibitors, particularly baricitinib and ruxolitinib in COVID-19[109,110]. In May 2022, the FDA approved a new indication for baricitinib in hospitalized adults with COVID-19 who require oxygen support. Notably, baricitinib exhibited significance against four disease signatures, while ruxolitinib showed significance across all seven disease signatures in our study. Tofacitinib, also identified by TReD, is recommended as an alternative option by the NIH in cases where baricitinib is not available[111]. Over half of the drugs in our results are substantiated by existing studies, supporting their relevance to COVID-19. For T2D, almost 40% (34/86) of the identified drugs have been previously studied and are linked to maintaining blood glucose homeostasis or slowing down the occurrence or progression of T2D. Among these drugs, we have highlighted liraglutide and miglitol, which are approved by the FDA and CFDA, respectively, for first-line treatment of T2D. Collectively, these results demonstrate the ability of the TReD framework to identify drug repositioning candidates.

The strengths of our framework stem from several key aspects. Firstly, the amalgamation of single-target and multiple-target approaches enables a more comprehensive therapeutic search, and this is particularly valuable for addressing complex diseases involving multiple biomolecules or mechanisms. Secondly, the framework incorporates two complementary methods (DGE and TWAS) as population-level sources for disease signatures. Although TWAS may be underpowered with a limited sample size, a critical feature of such a genetics-anchored method ensures that it identifies *potentially* regulatory or candidate causal genes for the disease, rather than genes altered by the disease. In contrast, DGE is prone to identify the transcriptomic consequences of the disease;

nevertheless, it remains well-powered even with limited sample sizes. The combination of these two methods should enrich for upstream mediators and molecular consequences, facilitating the discovery of new drug indications or the repositioning of existing drugs. Thirdly, the use of the reversal distance measurement in our study capitalizes on available (and growing) information from transcriptome-level disease-associated gene features and drug profiles, with biologically relevant interpretation of an effective therapeutic effect on disease. This differs from previous and, we would argue, less interpretable methods, such as those that have relied solely on a non-parametric KS statistic, focusing on the maximum difference in the relative ranks of the upregulated and downregulated genes[112]. Fourthly, we leveraged the latest CMAP LINCS 2020 data which contains over three million gene expression profiles with > 80,000 perturbations and > 200 cell lines affecting over 12,328 genes, providing a comprehensive candidate pool for drug repositioning. While our study focused on COVID-19 and T2D, our framework is highly generalizable and can be implemented to identify drug repositioning candidates for other diseases.

The limitations of the framework should also be acknowledged. Firstly, limited by data availability, only the transcriptome was considered. Comprehensive data from other omics disciplines for COVID-19 and T2D are currently lacking or, at best, remain very limited. Secondly, our study does not consider the highly complex issues of drug-target interactions and drug-drug interactions. Thirdly, i*n vivo* and *in vitro* drug responses may be significantly different, and indeed the actual therapeutic efficacy is likely to be far more multifaceted than the simple alignment of transcriptome profiles. In *vivo* drug responses are influenced by complex factors like pharmacokinetics and pharmacodynamics, which may not be easily aligned with *in vitro* observations. Despite these limitations, it should be noted that the TReD statistical methodology is sufficiently flexible to

integrate related methodological improvements, involving other types of omics data, more complex therapeutic profiles, and more realistic *in vivo* pharmacologic models.

In summary, integrating transcriptome-level profiles from cell-based response profiles and population-based disease signature studies, we developed a framework, TReD, to identify drug repurposing candidates. In practice, we successfully identified well-studied candidates and several other promising candidate drugs, such as Enzastaurin for COVID-19 treatment and caffeine for T2D prevention. The framework demonstrates effectiveness in drug repositioning and is highly applicable across various diseases.

STAR Methods

GWAS for COVID-19 severity

The GWAS summary statistics for COVID-19 severity were downloaded from COVID-19 Host Genetics Initiative (https://www.covid19hg.org/), the latest version, release 7 of the hospitalized versus population data. The hospitalized phenotype includes patients who were hospitalized with a laboratory-confirmed SARS-Cov2 infection. This dataset contains 44,989 cases and 2,356,386 controls. The summary statistics of GWAS of T2D were obtained from Xue et al's study, containing 62,892 T2D cases and 596,424 controls of European ancestry[113]. (http://cnsgenomics.com/data/t2d/Xue_et_al_T2D_META_Nat_Commun_2018.gz). Additional descriptions of the included studies can be found in Table S7.

TWAS and colocalization for COVID-19 severity and T2D

To identify diseaseassociated genes, we applied TWAS with the best prediction models among PrediXcan[114], UTMOST[115], and JTI[116] according to the prediction accuracy estimated by 5-fold

cross-validation. Briefly, the residuals of the normalized gene expression levels were used after regressing out covariates. SNPs within 1 Mb upstream and downstream of the gene body were considered as predictor variables in the models. Applying the prediction model to GWAS dataset, genetically predicted expression level was generated for each of the individuals. The significance for a gene was determined by a linear regression for estimating the association between predicted expression and trait. In practice, summary statistics-based association test was performed. Blood, lung, lymphocytes, and spleen were considered as relevant tissues for COVID-19. Visceral adipose, liver, pancreas, and skeletal muscle were considered relevant for T2D. For TWAS results that passed Bonferroni multiple testing correction, we performed colocalization to provide additional support under different sets of assumptions. To test colocalization in the presence of multiple causal variants, we applied coloc[117] to the signals decomposed by SuSiE[118] for each locus, including the variants located within ± 200 kb of the lead variant (*coloc-SuSiE*). Notably, *coloc-SuSiE* is more generalizable since it relaxes the "one causal variant" assumption of regular *coloc*. We used European participants in the 1000 genomes project as the LD reference. If SuSiE did not converge after 1000 iterations for either eQTL or GWAS summary statistics, we instead used the regular *coloc*. We considered that the signals of eQTL and GWAS were colocalized if the maximum posterior probability of colocalization (i.e., PP.H4 for *coloc* and *coloc-SuSiE*) was equal or larger than 0.85 either using *coloc* or *coloc-SuSiE*. TWAS significant genes showing positive colocalization evidence were then used to search for drugs targeting the genes, via DrugBank, TTD, DGIdb. DrugBank is a comprehensive and up-to-date resource for searching over 500,000 drugs and drug products, their targets, pathways, indications, and pharmacology. TTD is a comprehensive database of therapeutic targets, drugs, biomarkers and scaffolds for various diseases and ICD identifiers. DGIdb is a web resource that provides information

on drug-gene interactions and druggable genes from publications, databases, and other web-based sources.

DGE for COVID19 and T2D

In COVID-19, the DGE data (three independent gene expression signatures labeled 'ALV', 'EXP', 'BALF') are directly derived from the study of Brian L. Le et al[23]. The ALV signature was generated using RNA-seq in human adenocarcinomic alveolar basal epithelial cells infected with SARS-CoV-2 propagated from Vero E6 cells (GSE147507, 67 samples)[119] (Table S8). After Benjamini-Hochberg adjustment, there were 120 differentially expressed genes (DEGs) remaining——100 upregulated and 20 downregulated. The EXP signature was obtained by RNA-seq on organoid samples [120] (Table S9). These samples were grown in a medium with a Wnt surrogate supplement and infected with SARS-CoV-2 propagated from Vero E6 cells (GSE149312, 22 samples). After Benjamini-Hochberg adjustment and applying a fold-change cutoff (|log2 FC| > 2), 125 genes remained significant. The BALF signature was estimated by RNA-seq analysis of the bronchoalveolar lavage fluid samples from two COVID-19 patients (two samples per patient) and three healthy controls[121]. Brian L. Le et al used their raw counts as inputs to DESeq2 (v.1.24.0 R package) to call differentially expressed genes (DEGs). After adjusting for the sequencing platform, the default settings of DESeq2 were used. Retaining only protein-coding genes and applying both a significance threshold and a fold-change cutoff (FDR < 0.05, |log2 FC| > 4), 1349 genes were obtained to be used as the BALF signature (Table S10).

Three DGE datasets (labeled as 'islets', 'myoblasts', and 'myotubes') were included in the T2D analysis. The islet signature was derived from oligonucleotide microarrays of pancreatic islets isolated from humans with type 2 diabetes versus normal glucose-tolerant controls[122]. cRNA was hybridized to

Affymetrix U133A and B microarrays. 370 showed differences in expression at the $p < 0.01$ level(Table S11). The other two signatures were originated from the study of Davegårdh C et al[123]. They isolated human muscle stem cells (satellite cells) from vastus lateralis from 14 controls with normal glucose tolerance (NGT) and 14 individuals with T2D, and after isolation, satellite cells were expanded and differentiated from myoblasts into myotubes. mRNA expression data were obtained using HumanHT-12 Expression BeadChip (Illumina, San Diego, CA, USA) which targets 28,688 well-annotated transcripts. Data were background-corrected, log2-transformed, quantile-normalized, and batch-corrected using COMBAT. Based on a false discovery rate (FDR) below 5% ($q < 0.05$), 577 unique genes with differential expression were identified in myoblasts and 42 unique genes in myotubes (Table S12 and Table S13)

The CMAP LINCS 2020 dataset

The Library of Integrated Network-Based Cellular Signatures (LINCS) is a program funded by the NIH Common Fund. Its primary goal is to generate a large-scale and comprehensive catalog of perturbation-response signatures by utilizing a diverse collection of perturbations across many model systems and assay types. The CMAP LINCS 2020 data contains ~3 million gene expression profiles of instances which are defined as changes in the assay readout of a perturbed sample when compared to a control sample involving the perturbation reagents (e.g., small molecules, sgRNAs, shRNAs, antibodies and disease states) and model system reagents (cell lines, iPSCs, differentiated cells, and primary cells). Here, we mainly focused on the transcriptomic response to small-molecule perturbations in immune-related cells and blood glucose metabolism-related tissues for the application of the TReD methodology to COVID-19 and T2D, respectively. We downloaded the level 5 beta data consisting of gene expression response profiles arising from small-molecule perturbations from

CMAP LINCS 2020 (https://s3.amazonaws.com/macchiato.clue.io/builds/LINCS2020/level5/level5_beta_trt_cp_n720216x12328.gctx),

Evaluation of the reversal potential of candidate drugs

To quantify the extent of reversal on disease of a specific drug, we used the cosine similarity metric. For a given disease, we first represent the set of disease signatures as a vector in a high-dimensional space (whose dimension n is the total number of genes) with each nonzero element of the vector given by a disease-associated gene. The disease signatures can be derived from either TWAS or DGE. The vector for each candidate drug is embedded in the same n-dimensional space. For each disease signature vector and drug response pair, we compute the reversal distance. Let $\overrightarrow{G}$ denote a disease signature vector, $\overrightarrow{D}$ a drug profile vector, and rd the reversal distance. The rd quantifies the potential effect of the drug in reversing the disease signatures:

$$\omega := \cos\theta = \frac{\overrightarrow{G} \cdot \overrightarrow{D}}{\left|\left|\overrightarrow{G}\right|\right| \left|\left|\overrightarrow{D}\right|\right|} \qquad (1)$$

$$rd = \left|\left|\overrightarrow{G}\right|\right| \cos(\pi - \theta) \qquad (2)$$

Here, $||\vec{a}|| = \sqrt{\vec{a} \cdot \vec{a}}$ denotes the Euclidean norm of the vector $\vec{a}$. Note that the cosine similarity ω (equation 1) always lies in $[-1,1]$, with -1 indicating exactly opposite orientation of the disease signature and the drug response profile and +1 indicating parallel orientation. The change in ω in response to a perturbation in the i-th element of the drug response profile $\vec{D}$, d_i, or the i-th element of the gene signature $\vec{G}$, g_i, is given by:

$$\frac{\partial \omega}{\partial d_i} = \frac{g_i}{\left|\left|\overrightarrow{G}\right|\right| \left|\left|\overrightarrow{D}\right|\right|} - \frac{d_i(\overrightarrow{G} \cdot \overrightarrow{D})}{\left|\left|\overrightarrow{G}\right|\right| \left|\left|\overrightarrow{D}\right|\right|^3}$$

$$\frac{\partial \omega}{\partial g_i} = \frac{d_i}{\left\|\overrightarrow{G}\right\| \left\|\overrightarrow{D}\right\|} - \frac{g_i(\overrightarrow{G} \,.\, \overrightarrow{D})}{\left\|\overrightarrow{D}\right\| \left\|\overrightarrow{G}\right\|^3}$$

Each quantity measures the sensitivity of the metric. In equation 2, θ, and thus the reversal distance rd, is a function of $\overrightarrow{G}$ and $\overrightarrow{D}$. When we wish to emphasize this dependence, we will write rd as $rd(\overrightarrow{G}, \overrightarrow{D})$. Equation 2 defines a function:

$$d\left(\overrightarrow{G}, \overrightarrow{D}\right) = \frac{2\arccos(rd(\overrightarrow{G}, \overrightarrow{D}) / \left\|\overrightarrow{G}\right\|)}{\pi},$$

which satisfies the conditions for a distance function, namely, non-negativity: $d\left(\vec{a}, \vec{b}\right) \geq 0$; symmetry: $d\left(\vec{a}, \vec{b}\right) = d\left(\vec{b}, \vec{a}\right)$; the triangle inequality; and the coincidence axiom: $d\left(\vec{a}, \vec{b}\right) = 0$ if and only if $\vec{a} = \vec{b}$. Despite the symmetry of the distance function, there is clearly an underlying *asymmetry*, as the disease signature vector $\overrightarrow{G}$ determines which genes are the "relevant" elements of the drug response profile vector $\overrightarrow{D}$.

Of interest to us is the sampling distribution of the cosine similarity ω. Consider the function $h(s, t, u) = \frac{s}{\sqrt{tu}}$. Note that ω is equal to $h\left(\vec{G} \,.\, \vec{D},\ \vec{G} \,.\, \vec{G},\ \vec{D} \,.\, \vec{D}\right)$. Furthermore, $\vec{G} \,.\, \vec{G}$ and $\vec{D} \,.\, \vec{D}$ are $\chi^2(n)$ distributed. We leverage the so-called Delta Method. Using the first two terms of the Taylor series expansion and setting $\Gamma = (s, t, u)$ with expected value $\gamma = \mathrm{E}[\Gamma]$, we obtain approximate expressions for the mean and variance of $h(\Gamma)$:

$$\mathrm{E}[h(\Gamma)] \approx h(\gamma) + \nabla h(\gamma)^T \,.\, \mathrm{E}[\Gamma - \gamma]$$

$$\mathrm{Var}\left(h(\Gamma)\right) \approx \nabla h(\gamma)^T \,.\, \mathrm{Cov}(\Gamma) \,.\, \nabla h(\gamma)$$

where ∇h is the gradient.

In this framework, drug repurposing is a search problem: the vector $\overrightarrow{G}$ is evaluated against all possible $\overrightarrow{D}$, which are prioritized using rd. A larger rd indicates a stronger reversal effect. Assuming K total number of drugs tested and the reversal distance for the i-th drug, $rd(\overrightarrow{G}, \overrightarrow{D_i})$, we

get a probability distribution consisting of the K probabilities p_i conditional on the disease signature information:

$$p_i = P\left(\overrightarrow{D_i} \middle| \overrightarrow{G}\right) = \frac{\exp\left(rd(\overrightarrow{G}, \overrightarrow{D_i})\right)}{\sum_{j=1}^{K} \exp\left(rd(\overrightarrow{G}, \overrightarrow{D_j})\right)}$$

by applying the softmax function. One drug repurposing approach is to identify the drug that maximizes the reversal distance:

$$\mathrm{D}^* = \underset{\vec{D}}{\operatorname{argmax}}\left(\ln\left(\left|\left|\overrightarrow{G}\right|\right|\right) + \ln\left(\cos\left(\pi - \theta(\overrightarrow{G}, \overrightarrow{D})\right)\right)\right)$$

Here, we instead prioritized a potentially larger set of drugs, i.e., the top candidates that meet a significance threshold.

We converted the gene-disease association signals into rank ratios, which, for each gene, is defined as the rank of the gene divided by the total number of genes. Similarly, each element of the drug response profile was set to the rank-transformed cell-based drug-induced gene expression response.

We performed a test of significance of each candidate drug. For each drug profile, a p-value for the reversal distance is estimated by permutation. For each permutation, the rank ratios are randomly shuffled, and the corresponding null reversal distance is computed. This process constructs an empirical null distribution of reversal distance for each drug. Subsequently, for each drug, we calculated the probability that the empirical reversal distance could have originated from the null distribution of the reversal distance. This involved counting the number of null reversal distance values greater than the real reversal distance and dividing this count by the total number of permutations to generate an empirical p-value. Drugs showing significance in the permutation test ($P < 0.05$) and large rd (over 2 standard deviations from the mean across the tested drugs) are defined

as strong candidates.

We also implemented a degree-preserving permutation approach. Let $G = (V, E)$ be a graph, where V is the set of nodes (genes) and E is the set of edges (defined by a co-expression network in a given tissue). To generate a permutation which preserves the degree distribution of the network, we randomly select two edges (say, $a \leftrightarrow b$ and $c \leftrightarrow d$) with non-overlapping nodes, remove the edges between the nodes, and create new edges ($a \leftrightarrow c$ and $b \leftrightarrow d$) by swapping the nodes until a certain proportion (80%) of the edges have been shuffled. The null reversal distance is computed for each such permutation.

Application of TReD to COVID-19 severity and T2D

Leveraging the TWAS/DGE results and the cell-based gene expression data from CMAP LINCS 2020, we implemented the TReD framework to identify drug repositioning candidates for COVID-19. Immune-related and T2D-related cell lines (matching the T2D-related tissues) have been annotated by multiple resources including the CMAP LINCS 2020 and the CCLE (cancer cell lines have been used to study COVID-19 and other diseases[124]). Information on drugs and drug targets is curated in the bioinformatics and chemoinformatics resource DrugBank (DrugBank Release Version 5.1.10 | DrugBank Online). In this study, 2,413 drugs and 12 immune-related cell types were included.

We leveraged the TWAS results of four tissues (blood, lung, lymphocytes, and spleen/visceral adipose, liver, pancreas, and skeletal muscle) and three DGE profiles as disease signatures (as defined in the previous section). Drug candidates were identified by permutation (1000 times sampling) and whether the reversal distance was greater than mean + 2 standard deviation. To ensure the robustness of the reversal relationship, we considered only those drugs whose reversal potential could be verified in additional cell line(s).

Data access

Links for databases and datasets used in this study: COVID-19 severity GWAS summary statistics: COVID19-hg GWAS meta-analyses round 7 (covid19hg.org); T2D GWAS summary statistics: http://cnsgenomics.com/data/t2d/Xue_et_al_T2D_META_Nat_Commun_2018.gz; CMAP LINCS 2020: https://s3.amazonaws.com/macchiato.clue.io/builds/LINCS2020/level5/level5_beta_trt_cp_n720216x12328.gctx; CCLE: Cancer Cell Line Encyclopedia (CCLE) (broadinstitute.org); DrugBank Release Version 5.1.10: DrugBank Release Version 5.1.10 | DrugBank Online; The used scripts are available at https://github.com/zdangm/TReD.

Competing interest statement

The authors declare no competing interests.

Acknowledgments

This research is supported by the Fundamental Research Funds from the Central Universities of Zhejiang University (D.Z.), the National Natural Sciences Foundation of China 82204118 (D.Z.), the National Institutes of Health (NIH) Genomic Innovator Award R35HG010718 (E.R.G.), NIH/NHGRI R01HG011138 (E.R.G.), NIH/NIA R56AG068026 (E.R.G.), and NIH/NIGMS R01GM140287 (E.R.G.).

Author contributions

Conceptualization, Dan Zhou and Eric R. Gamazon; formal analysis, Chunfeng He, Yue Xu, Yuan

Zhou, and Ran Meng; writing--original draft, Chunfeng He, and Yue Xu; writing--review & editing, Dan Zhou, Eric R. Gamazon, Yuan Zhou, Jiayao Fan, Chunxiao Cheng, and Lang Wu.

ReferencesUncategorized References

1. Wouters, O.J., McKee, M. & Luyten, J. Estimated Research and Development Investment Needed to Bring a New Medicine to Market, 2009-2018. *Jama* **323**, 844-853 (2020).
2. DiMasi, J.A., Hansen, R.W. & Grabowski, H.G. The price of innovation: new estimates of drug development costs. *J Health Econ* **22**, 151-85 (2003).
3. King, E.A., Davis, J.W. & Degner, J.F. Are drug targets with genetic support twice as likely to be approved? Revised estimates of the impact of genetic support for drug mechanisms on the probability of drug approval. *PLoS Genet* **15**, e1008489 (2019).
4. Nelson, M.R. *et al.* The support of human genetic evidence for approved drug indications. *Nat Genet* **47**, 856-60 (2015).
5. Pairo-Castineira, E. *et al.* Genetic mechanisms of critical illness in COVID-19. *Nature* **591**, 92-98 (2021).
6. Marconi, V.C. *et al.* Efficacy and safety of baricitinib for the treatment of hospitalised adults with COVID-19 (COV-BARRIER): a randomised, double-blind, parallel-group, placebo-controlled phase 3 trial. *Lancet Respir Med* **9**, 1407-1418 (2021).
7. Kalil, A.C. *et al.* Baricitinib plus Remdesivir for Hospitalized Adults with Covid-19. *N Engl J Med* **384**, 795-807 (2021).
8. Baricitinib in patients admitted to hospital with COVID-19 (RECOVERY): a randomised,

593 controlled, open-label, platform trial and updated meta-analysis. *Lancet* **400**, 359-368 (2022).

594 9. Houghten, R.A. *et al.* Mixture-based synthetic combinatorial libraries. *J Med Chem* **42**,

595 3743-78 (1999).

596 10. Paolini, G.V., Shapland, R.H., van Hoorn, W.P., Mason, J.S. & Hopkins, A.L. Global mapping

597 of pharmacological space. *Nat Biotechnol* **24**, 805-15 (2006).

598 11. Hopkins, A.L. Network pharmacology: the next paradigm in drug discovery. *Nat Chem Biol* **4**,

599 682-90 (2008).

600 12. Chen, B. *et al.* Computational Discovery of Niclosamide Ethanolamine, a Repurposed Drug

601 Candidate That Reduces Growth of Hepatocellular Carcinoma Cells In Vitro and in Mice by

602 Inhibiting Cell Division Cycle 37 Signaling. *Gastroenterology* **152**, 2022-2036 (2017).

603 13. Chen, B. *et al.* Reversal of cancer gene expression correlates with drug efficacy and reveals

604 therapeutic targets. *Nat Commun* **8**, 16022 (2017).

605 14. Porcu, E. *et al.* Differentially expressed genes reflect disease-induced rather than

606 disease-causing changes in the transcriptome. *Nat Commun* **12**, 5647 (2021).

607 15. Barbeira, A.N. *et al.* Exploring the phenotypic consequences of tissue specific gene

608 expression variation inferred from GWAS summary statistics. *Nat Commun* **9**, 1825 (2018).

609 16. Pilarczyk, M., Najafabadi, M.F., Kouril, M., Vasiliauskas, J. & Medvedovic, M. Connecting

610 omics signatures of diseases, drugs, and mechanisms of actions with iLINCS. (2019).

611 17. Subramanian, A. *et al.* A Next Generation Connectivity Map: L1000 Platform and the First

612 1,000,000 Profiles. *Cell* **171**, 1437-1452.e17 (2017).

613 18. Lamb, J. *et al.* The Connectivity Map: using gene-expression signatures to connect small

614 molecules, genes, and disease. *Science* **313**, 1929-35 (2006).

615 19. Hu, R.Y. *et al.* Individualized Drug Repositioning For Rheumatoid Arthritis Using Weighted
616 Kolmogorov-Smirnov Algorithm. *Pharmgenomics Pers Med* **12**, 369-375 (2019).
617 20. Pushpakom, S. *et al.* Drug repurposing: progress, challenges and recommendations. *Nat Rev*
618 *Drug Discov* **18**, 41-58 (2019).
619 21. Reay, W.R. & Cairns, M.J. Advancing the use of genome-wide association studies for drug
620 repurposing. *Nat Rev Genet* **22**, 658-671 (2021).
621 22. Wagner, A. *et al.* Drugs that reverse disease transcriptomic signatures are more effective in a
622 mouse model of dyslipidemia. *Mol Syst Biol* **11**, 791 (2015).
623 23. Le, B.L. *et al.* Transcriptomics-based drug repositioning pipeline identifies therapeutic
624 candidates for COVID-19. *Sci Rep* **11**, 12310 (2021).
625 24. Vanderbeke, L. *et al.* Monocyte-driven atypical cytokine storm and aberrant neutrophil
626 activation as key mediators of COVID-19 disease severity. *Nat Commun* **12**, 4117 (2021).
627 25. Wishart, D.S. *et al.* DrugBank 5.0: a major update to the DrugBank database for 2018. *Nucleic*
628 *Acids Res* **46**, D1074-d1082 (2018).
629 26. Freshour, S.L. *et al.* Integration of the Drug-Gene Interaction Database (DGIdb 4.0) with open
630 crowdsource efforts. *Nucleic Acids Res* **49**, D1144-d1151 (2021).
631 27. Zhou, Y. *et al.* Therapeutic target database update 2022: facilitating drug discovery with
632 enriched comparative data of targeted agents. *Nucleic Acids Res* **50**, D1398-d1407 (2022).
633 28. Horby, P. *et al.* Dexamethasone in Hospitalized Patients with Covid-19. *N Engl J Med* **384**,
634 693-704 (2021).
635 29. Li, B. *et al.* Genome-wide CRISPR screen identifies host dependency factors for influenza A
636 virus infection. *Nat Commun* **11**, 164 (2020).

637 30. Pairo-Castineira, E. *et al.* GWAS and meta-analysis identifies 49 genetic variants underlying
638 critical COVID-19. *Nature* **617**, 764-768 (2023).
639 31. Muhammad, J.S., Siddiqui, R. & Khan, N.A. COVID-19: Is There a Link between Alcohol
640 Abuse and SARS-CoV-2-Induced Severe Neurological Manifestations? *ACS Pharmacol*
641 *Transl Sci* **4**, 1024-1025 (2021).
642 32. Wang, L. *et al.* An atlas connecting shared genetic architecture of human diseases and
643 molecular phenotypes provides insight into COVID-19 susceptibility. *Genome Med* **13**, 83
644 (2021).
645 33. Cao, H., Baranova, A., Song, Y., Chen, J.H. & Zhang, F. Causal associations and genetic
646 overlap between COVID-19 and intelligence. *Qjm* (2023).
647 34. Wu, L., Zhu, J., Liu, D., Sun, Y. & Wu, C. An integrative multiomics analysis identifies putative
648 causal genes for COVID-19 severity. *Genet Med* **23**, 2076-2086 (2021).
649 35. Ellinghaus, D. *et al.* Genomewide Association Study of Severe Covid-19 with Respiratory
650 Failure. *N Engl J Med* **383**, 1522-1534 (2020).
651 36. Ray, J.G., Schull, M.J., Vermeulen, M.J. & Park, A.L. Association Between ABO and Rh Blood
652 Groups and SARS-CoV-2 Infection or Severe COVID-19 Illness : A Population-Based Cohort
653 Study. *Ann Intern Med* **174**, 308-315 (2021).
654 37. Krishnamoorthy, S., Li, G.H. & Cheung, C.L. Transcriptome-wide summary data-based
655 Mendelian randomization analysis reveals 38 novel genes associated with severe COVID-19.
656 *J Med Virol* **95**, e28162 (2023).
657 38. Cui, H. & Zhang, L. Key Components of Inflammasome and Pyroptosis Pathways Are
658 Deficient in Canines and Felines, Possibly Affecting Their Response to SARS-CoV-2 Infection.

659 *Front Immunol* **11**, 592622 (2020).

660 39. Chang, J.J. *et al.* Long-Read RNA Sequencing Identifies Polyadenylation Elongation and
661 Differential Transcript Usage of Host Transcripts During SARS-CoV-2 In Vitro Infection. *Front*
662 *Immunol* **13**, 832223 (2022).

663 40. Banday, A.R. *et al.* Genetic regulation of OAS1 nonsense-mediated decay underlies
664 association with COVID-19 hospitalization in patients of European and African ancestries. *Nat*
665 *Genet* **54**, 1103-1116 (2022).

666 41. Zhu, Z. *et al.* An integrated strategy to identify COVID-19 causal genes and characteristics
667 represented by LRRC37A2. *J Med Virol* **95**, e28585 (2023).

668 42. Kousathanas, A. *et al.* Whole-genome sequencing reveals host factors underlying critical
669 COVID-19. *Nature* **607**, 97-103 (2022).

670 43. Andreakos, E. *et al.* A global effort to dissect the human genetic basis of resistance to
671 SARS-CoV-2 infection. *Nat Immunol* **23**, 159-164 (2022).

672 44. Yao, M., Huang, X., Guo, Y., Zhao, J.V. & Liu, Z. Disentangling the common genetic
673 architecture and causality of rheumatoid arthritis and systemic lupus erythematosus with
674 COVID-19 outcomes: Genome-wide cross trait analysis and bidirectional Mendelian
675 randomization study. *J Med Virol* **95**, e28570 (2023).

676 45. Zheng, J. *et al.* Multi-ancestry Mendelian randomization of omics traits revealing drug targets
677 of COVID-19 severity. *EBioMedicine* **81**, 104112 (2022).

678 46. Yao, Y. *et al.* Genome and epigenome editing identify CCR9 and SLC6A20 as target genes at
679 the 3p21.31 locus associated with severe COVID-19. *Signal Transduct Target Ther* **6**, 85
680 (2021).

681 47. Bagabir, S.A. Investigating the potential of natural compounds as novel inhibitors of
682 SARS-CoV-2 RdRP using computational approaches. *Biotechnol Genet Eng Rev*, 1-21
683 (2023).
684 48. Wang, X. *et al.* Astemizole as a drug to inhibit the effect of SARS-COV-2 in vitro. *Microb*
685 *Pathog* **156**, 104929 (2021).
686 49. Costanzo, M.C. *et al.* The Type 2 Diabetes Knowledge Portal: An open access genetic
687 resource dedicated to type 2 diabetes and related traits. *Cell Metab* **35**, 695-710.e6 (2023).
688 50. Mazziotti, G. *et al.* Outcome of glucose homeostasis in patients with glucocorticoid-induced
689 osteoporosis undergoing treatment with bone active-drugs. *Bone* **67**, 175-80 (2014).
690 51. D'Alessio, A. *et al.* Low-dose ruxolitinib plus steroid in severe SARS-CoV-2 pneumonia.
691 *Leukemia* **35**, 635-638 (2021).
692 52. Koschmieder, S. *et al.* Favorable COVID-19 course despite significant comorbidities in a
693 ruxolitinib-treated patient with primary myelofibrosis. *Eur J Haematol* **105**, 655-658 (2020).
694 53. Vannucchi, A.M. *et al.* Compassionate use of JAK1/2 inhibitor ruxolitinib for severe COVID-19:
695 a prospective observational study. *Leukemia* **35**, 1121-1133 (2021).
696 54. Han, M.K. *et al.* Ruxolitinib in addition to standard of care for the treatment of patients admitted
697 to hospital with COVID-19 (RUXCOVID): a randomised, double-blind, placebo-controlled,
698 phase 3 trial. *Lancet Rheumatol* **4**, e351-e361 (2022).
699 55. Rein, L. *et al.* Randomized Phase 3 Trial of Ruxolitinib for COVID-19-Associated Acute
700 Respiratory Distress Syndrome. *Crit Care Med* **50**, 1701-1713 (2022).
701 56. Ji, H.L. *et al.* SARS-CoV proteins decrease levels and activity of human ENaC via activation of
702 distinct PKC isoforms. *Am J Physiol Lung Cell Mol Physiol* **296**, L372-83 (2009).

703 57. Gupta, Y. *et al.* Bisindolylmaleimide IX: A novel anti-SARS-CoV2 agent targeting viral main
704 protease 3CLpro demonstrated by virtual screening pipeline and in-vitro validation assays.
705 *Methods* **195**, 57-71 (2021).
706 58. Huang, C. *et al.* Protein Kinase C Inhibitors Reduce SARS-CoV-2 Replication in Cultured Cells.
707 *Microbiol Spectr* **10**, e0105622 (2022).
708 59. Yassin, A. *et al.* Testosterone and Covid-19: An update. *Rev Med Virol* **33**, e2395 (2023).
709 60. Hempel, T. *et al.* Synergistic inhibition of SARS-CoV-2 cell entry by otamixaban and covalent
710 protease inhibitors: pre-clinical assessment of pharmacological and molecular properties.
711 *Chem Sci* **12**, 12600-12609 (2021).
712 61. Poole, R. *et al.* Coffee consumption and health: umbrella review of meta-analyses of multiple
713 health outcomes. *Bmj* **359**, j5024 (2017).
714 62. Larsson, S.C., Woolf, B. & Gill, D. Appraisal of the causal effect of plasma caffeine on
715 adiposity, type 2 diabetes, and cardiovascular disease: two sample mendelian randomisation
716 study. *BMJ Med* **2**, 1-8 (2023).
717 63. Li, Z. *et al.* Inhibition of Epidermal Growth Factor Receptor Activation Is Associated With
718 Improved Diabetic Nephropathy and Insulin Resistance in Type 2 Diabetes. *Diabetes* **67**,
719 1847-1857 (2018).
720 64. Veneri, D., Franchini, M. & Bonora, E. Imatinib and regression of type 2 diabetes. *N Engl J*
721 *Med* **352**, 1049-50 (2005).
722 65. Han, M.S. *et al.* Imatinib mesylate reduces endoplasmic reticulum stress and induces
723 remission of diabetes in db/db mice. *Diabetes* **58**, 329-36 (2009).
724 66. Al Batran, R. *et al.* Pimozide Alleviates Hyperglycemia in Diet-Induced Obesity by Inhibiting

725 Skeletal Muscle Ketone Oxidation. *Cell Metab* **31**, 909-919.e8 (2020).

726 67. Harrison, A.V., Lorenzo, F.R. & McClain, D.A. Iron and the Pathophysiology of Diabetes. *Annu*
727 *Rev Physiol* **85**, 339-362 (2023).

728 68. Jiang, Y. *et al.* Insights into potential mechanisms of asthma patients with COVID-19: A study
729 based on the gene expression profiling of bronchoalveolar lavage fluid. *Comput Biol Med* **146**,
730 105601 (2022).

731 69. Bharadwaj, S. *et al.* SARS-CoV-2 M(pro) inhibitors: identification of anti-SARS-CoV-2 M(pro)
732 compounds from FDA approved drugs. *J Biomol Struct Dyn* **40**, 2769-2784 (2022).

733 70. Sinha, S. *et al.* In vitro and in vivo identification of clinically approved drugs that modify ACE2
734 expression. *Mol Syst Biol* **16**, e9628 (2020).

735 71. Guimarães, P.O. *et al.* Tofacitinib in Patients Hospitalized with Covid-19 Pneumonia. *N Engl J*
736 *Med* **385**, 406-415 (2021).

737 72. Kaliamurthi, S. *et al.* Structure-Based Virtual Screening Reveals Ibrutinib and Zanubrutinib as
738 Potential Repurposed Drugs against COVID-19. *Int J Mol Sci* **22**(2021).

739 73. Bischof, E., Siow, R.C., Zhavoronkov, A. & Kaeberlein, M. The potential of rapalogs to
740 enhance resilience against SARS-CoV-2 infection and reduce the severity of COVID-19.
741 *Lancet Healthy Longev* **2**, e105-e111 (2021).

742 74. Xie, J. *et al.* Inhibition of MEK signaling prevents SARS-CoV2-induced lung damage and
743 improves the survival of infected mice. *J Med Virol* **94**, 6097-6102 (2022).

744 75. Lamontagne, F. *et al.* A living WHO guideline on drugs for covid-19. *Bmj* **370**, m3379 (2020).

745 76. Bahrami, M., Kamalinejad, M., Latifi, S.A., Seif, F. & Dadmehr, M. Cytokine storm in COVID-19
746 and parthenolide: Preclinical evidence. *Phytother Res* **34**, 2429-2430 (2020).

747 77. Preet, G., Oluwabusola, E.T., Milne, B.F., Ebel, R. & Jaspars, M. Computational Repurposing
748 of Mitoxantrone-Related Structures against Monkeypox Virus: A Molecular Docking and 3D
749 Pharmacophore Study. *Int J Mol Sci* **23**(2022).
750 78. Drayman, N. *et al.* Masitinib is a broad coronavirus 3CL inhibitor that blocks replication of
751 SARS-CoV-2. *Science* **373**, 931-936 (2021).
752 79. von Metzler, I. *et al.* COVID-19 in multiple-myeloma patients: cellular and humoral immunity
753 against SARS-CoV-2 in a short- and long-term view. *J Mol Med (Berl)* **100**, 463-470 (2022).
754 80. Saul, S. *et al.* Anticancer pan-ErbB inhibitors reduce inflammation and tissue injury and exert
755 broad-spectrum antiviral effects. *J Clin Invest* (2023).
756 81. van de Veerdonk, F.L. *et al.* A guide to immunotherapy for COVID-19. *Nat Med* **28**, 39-50
757 (2022).
758 82. Wang, W. *et al.* Gossypol Broadly Inhibits Coronaviruses by Targeting RNA-Dependent RNA
759 Polymerases. *Adv Sci (Weinh)* **9**, e2203499 (2022).
760 83. Colmenero, J. *et al.* Epidemiological pattern, incidence, and outcomes of COVID-19 in liver
761 transplant patients. *J Hepatol* **74**, 148-155 (2021).
762 84. Sajid Jamal, Q.M., Alharbi, A.H. & Ahmad, V. Identification of doxorubicin as a potential
763 therapeutic against SARS-CoV-2 (COVID-19) protease: a molecular docking and dynamics
764 simulation studies. *J Biomol Struct Dyn* **40**, 7960-7974 (2022).
765 85. Ahmad, S. *et al.* Reporting dinaciclib and theodrenaline as a multitargeted inhibitor against
766 SARS-CoV-2: an in-silico study. *J Biomol Struct Dyn* **41**, 4013-4023 (2023).
767 86. Tomazou, M. *et al.* Multi-omics data integration and network-based analysis drives a multiplex
768 drug repurposing approach to a shortlist of candidate drugs against COVID-19. *Brief Bioinform*

769 **22**(2021).

770 87. Chen, T., Philip, M., KA, L.C. & Tyagi, S. A multi-modal data harmonisation approach for

771 discovery of COVID-19 drug targets. *Brief Bioinform* **22**(2021).

772 88. Li, T.W. *et al.* SARS-CoV-2 Nsp14 protein associates with IMPDH2 and activates NF-κB

773 signaling. *Front Immunol* **13**, 1007089 (2022).

774 89. Biji, A. *et al.* Identification of COVID-19 prognostic markers and therapeutic targets through

775 meta-analysis and validation of Omics data from nasopharyngeal samples. *EBioMedicine* **70**,

776 103525 (2021).

777 90. Repurposing Cancer Drugs for COVID-19. *Cancer Discov* **10**, Of2 (2020).

778 91. Nose, A. *et al.* Regulation of glucose transporter (GLUT1) gene expression by angiotensin II in

779 mesangial cells: involvement of HB-EGF and EGF receptor transactivation. *Hypertens Res* **26**,

780 67-73 (2003).

781 92. Ye, H., Yan, J., Wang, Q., Tian, H. & Zhou, L. The protective effects of cabozantinib against

782 high glucose-induced damages in in vitro renal glomerular endothelial cells model via inhibition

783 of early growth response-1 (Egr-1). *Bioengineered* **13**, 10605-10616 (2022).

784 93. Sharma, V. *et al.* Metoprolol improves cardiac function and modulates cardiac metabolism in

785 the streptozotocin-diabetic rat. *Am J Physiol Heart Circ Physiol* **294**, H1609-20 (2008).

786 94. Glaser, N., Yuen, N., Anderson, S.E., Tancredi, D.J. & O'Donnell, M.E. Cerebral metabolic

787 alterations in rats with diabetic ketoacidosis: effects of treatment with insulin and intravenous

788 fluids and effects of bumetanide. *Diabetes* **59**, 702-9 (2010).

789 95. Neri Serneri, G.G., Coccheri, S., Marubini, E. & Violi, F. Picotamide, a combined inhibitor of

790 thromboxane A2 synthase and receptor, reduces 2-year mortality in diabetics with peripheral

791 arterial disease: the DAVID study. *Eur Heart J* **25**, 1845-52 (2004).

792 96. Bele, S. *et al.* MS-275, a class 1 histone deacetylase inhibitor augments glucagon-like
793 peptide-1 receptor agonism to improve glycemic control and reduce obesity in diet-induced
794 obese mice. *Elife* **9**(2020).

795 97. Mothe-Satney, I. *et al.* Adipocytes secrete leukotrienes: contribution to obesity-associated
796 inflammation and insulin resistance in mice. *Diabetes* **61**, 2311-9 (2012).

797 98. Resmi, H. The combination of bortezomib and resveratrol may prevent muscle wasting in
798 diabetes. *Med Hypotheses* **76**, 291-2 (2011).

799 99. Samaha, M.M., Helal, M.G., El-Sherbiny, M., Said, E. & Salem, H.A. Indapamide Increases
800 IRS1 Expression and Modifies Adiponectin/NLRP3/PPARγ Crosstalk in Type 2 Diabetic Rats.
801 *Antioxidants (Basel)* **11**(2022).

802 100. Ullah, A. *et al.* Insulinotropic Potential of Moxifloxacin and Gemifloxacin: An In Vivo Rabbits
803 Model Study Followed by Randomized Phase I Clinical Trial. *Antibiotics (Basel)* **11**(2022).

804 101. Liang, L., Beshay, E. & Prud'homme, G.J. The phosphodiesterase inhibitors pentoxifylline and
805 rolipram prevent diabetes in NOD mice. *Diabetes* **47**, 570-5 (1998).

806 102. Ayalasomayajula, S.P. & Kompella, U.B. Subconjunctivally administered celecoxib-PLGA
807 microparticles sustain retinal drug levels and alleviate diabetes-induced oxidative stress in a
808 rat model. *Eur J Pharmacol* **511**, 191-8 (2005).

809 103. Urtado, C.B. *et al.* Resistance training associated with the administration of
810 anabolic-androgenic steroids improves insulin sensitivity in ovariectomized rats. *Diabetes*
811 *Metab Syndr Obes* **4**, 385-91 (2011).

812 104. Akindele, A.J., Otuguor, E., Singh, D., Ota, D. & Benebo, A.S. Hypoglycemic, antilipidemic and

813 antioxidant effects of valproic acid in alloxan-induced diabetic rats. *Eur J Pharmacol* **762**,
814 174-83 (2015).
815 105. Trivedi, P.M. *et al.* Repurposed JAK1/JAK2 Inhibitor Reverses Established Autoimmune
816 Insulitis in NOD Mice. *Diabetes* **66**, 1650-1660 (2017).
817 106. Tay, M.Z., Poh, C.M., Rénia, L., MacAry, P.A. & Ng, L.F.P. The trinity of COVID-19: immunity,
818 inflammation and intervention. *Nat Rev Immunol* **20**, 363-374 (2020).
819 107. Merad, M., Blish, C.A., Sallusto, F. & Iwasaki, A. The immunology and immunopathology of
820 COVID-19. *Science* **375**, 1122-1127 (2022).
821 108. Lee, S. *et al.* Virus-induced senescence is a driver and therapeutic target in COVID-19. *Nature*
822 **599**, 283-289 (2021).
823 109. Wijaya, I. *et al.* The use of Janus Kinase inhibitors in hospitalized patients with COVID-19:
824 Systematic review and meta-analysis. *Clin Epidemiol Glob Health* **11**, 100755 (2021).
825 110. Patoulias, D., Doumas, M., Papadopoulos, C. & Karagiannis, A. Janus kinase inhibitors and
826 major COVID-19 outcomes: time to forget the two faces of Janus! A meta-analysis of
827 randomized controlled trials. *Clin Rheumatol* **40**, 4671-4674 (2021).
828 111. in *Coronavirus Disease 2019 (COVID-19) Treatment Guidelines* (National Institutes of Health
829 (US), Bethesda (MD), 2021).
830 112. Sirota, M. *et al.* Discovery and preclinical validation of drug indications using compendia of
831 public gene expression data. *Sci Transl Med* **3**, 96ra77 (2011).
832 113. Xue, A. *et al.* Genome-wide association analyses identify 143 risk variants and putative
833 regulatory mechanisms for type 2 diabetes. *Nat Commun* **9**, 2941 (2018).
834 114. Gamazon, E.R. *et al.* A gene-based association method for mapping traits using reference

835 transcriptome data. *Nature Genetics* **47**, 1091-1098 (2015).

836 115. Hu, Y. *et al.* A statistical framework for cross-tissue transcriptome-wide association analysis.

837 *Nature Genetics* **51**, 568-576 (2019).

838 116. Zhou, D. *et al.* A unified framework for joint-tissue transcriptome-wide association and

839 Mendelian randomization analysis. *Nat Genet* **52**, 1239-1246 (2020).

840 117. Giambartolomei, C. *et al.* Bayesian test for colocalisation between pairs of genetic association

841 studies using summary statistics. *PLoS Genet* **10**, e1004383 (2014).

842 118. Wallace, C. A more accurate method for colocalisation analysis allowing for multiple causal

843 variants. *PLoS Genet* **17**, e1009440 (2021).

844 119. Blanco-Melo, D. *et al.* Imbalanced Host Response to SARS-CoV-2 Drives Development of

845 COVID-19. *Cell* **181**, 1036-1045.e9 (2020).

846 120. Lamers, M.M. *et al.* SARS-CoV-2 productively infects human gut enterocytes. *Science* **369**,

847 50-54 (2020).

848 121. Xiong, Y. *et al.* Transcriptomic characteristics of bronchoalveolar lavage fluid and peripheral

849 blood mononuclear cells in COVID-19 patients. *Emerg Microbes Infect* **9**, 761-770 (2020).

850 122. Gunton, J.E. *et al.* Loss of ARNT/HIF1beta mediates altered gene expression and

851 pancreatic-islet dysfunction in human type 2 diabetes. *Cell* **122**, 337-49 (2005).

852 123. Davegårdh, C. *et al.* VPS39-deficiency observed in type 2 diabetes impairs muscle stem cell

853 differentiation via altered autophagy and epigenetics. *Nat Commun* **12**, 2431 (2021).

854 124. Bakowski, M.A. *et al.* Drug repurposing screens identify chemical entities for the development

855 of COVID-19 interventions. *Nat Commun* **12**, 3309 (2021).

856